



# Modification of optical and mechanical properties of nitrogen doped diamond-like carbon layers

R. Zarei Moghadam<sup>1</sup> · H. Rezagholipour Dizaji<sup>1</sup> · M. H. Ehsani<sup>1</sup>

Received: 4 May 2019 / Accepted: 4 October 2019 / Published online: 14 October 2019  
© Springer Science+Business Media, LLC, part of Springer Nature 2019

## Abstract

We have deposited diamond-like carbon (DLC) films on glass and Si substrates with direct ion beam deposition technique and investigated the effect of N<sub>2</sub> doping on their structural, mechanical, and optical properties. The DLC coatings were doped with nitrogen under different flow rates of 5, 10, 20, 40, and 50 sccm. Morphological characteristics investigation of the prepared samples showed decrement in their average roughness from 4.1 to 0.68 nm. Raman studies showed that the number of graphitic sp<sup>2</sup> bonding increased with N doping. By increasing the N<sub>2</sub> content, the graphite cluster size increased. FTIR measurement revealed the functional groups available in the prepared samples. UV–Vis analysis showed that the optical transmission of nitrogen-doped DLC (N-DLC) coatings decreased when N<sub>2</sub> content increased from 5 to 40 sccm followed by decrement in both the optical band gap and the internal stress. Finally, the mechanical properties such as hardness and elastic modulus decreased by increasing N<sub>2</sub> content from 5 to 40 sccm.

## 1 Introduction

Diamond-like carbon (DLC) films have attracted the attention of many researchers due to their combined properties of graphite and diamond such as high hydrophobicity and hardness, wear resistance, and good optical coefficient among the other characteristics [1–5]. DLC thin films are good candidates for a variety of applications, including a protective cover on anti-reflection coating, solar cells, biomedical devices, and memory storage ones [6–10]. To improve the properties such as optical, mechanical, and so on, many authors have studied the effects of doping DLC films by various elements such as O, Si, B, N, and Ag [11–15]. It is reported that by incorporating nitrogen into DLC coatings, the friction and internal stress of the film can be reduced [16, 17].

In DLC thin films, mechanical properties such as residual stress, depend mainly on the amount of sp<sup>3</sup> bonding, which is mainly under the influence of ion energy being equal to the growth parameters and dopant type [18–20]. Residual stress, present in DLC thin films, can be reduced via doping by various elements. Amongst different elements,

nitrogen has been widely studied as a dopant in DLC thin films, which helps to reduce the stress of DLC thin films [21]. When nitrogen is incorporated into a DLC thin film, C–N groups will take form and operation as an electron receiver due to their strong electron withdrawing capability is done [22]. Kopustinskas et al. studied  $\alpha$ -CN<sub>x</sub>:H films prepared with a ion beam deposition from C<sub>6</sub>H<sub>14</sub> + H<sub>2</sub> + N<sub>2</sub> gas mixture on Si (100) substrates and observed that, due to increasing nitrogen in the gas mixture, refractive index, growth rate, and sp<sup>3</sup> bonding decreased and there was more graphite-like formation [23]. Tsuchiya et al. reported the preparation of nitrogen-doped DLC (N-DLC) films with PECVD technique by CH<sub>4</sub>, N<sub>2</sub>, and Ar gases on Si substrate and also investigated the effect of N<sub>2</sub> incorporation on their structural, electrical, optical, and mechanical properties. They described that the internal stress of the prepared DLC samples was reduced (less than 0.5 GPa) by N doping at N<sub>2</sub> flow rates to less than 13.6% and the electrical resistivity decreased (less 10<sup>-2</sup> Ω cm) [24]. Lee et al. reported characteristics of N<sub>2</sub> incorporation into DLC thin films deposited with the unbalanced magnetron sputtering for electronic devices. The measured electrical resistivity of their DLC samples reduced while the hardness and elastic modulus of the samples increased with the amount of N<sub>2</sub> gas [25]. Jonas et al. reported stability of a-C:N:H layers deposited by RF plasma enhanced CVD method. They described that the temperature rise resulted in the deposition rate decrease. This

✉ H. Rezagholipour Dizaji  
hrgholipour@semnan.ac.ir

<sup>1</sup> Faculty of Physics, Semnan University, P.O. Box: 35195-363, Semnan, Islamic Republic of Iran

unfavorable effect may be reduced by application of increasing gas pressure and/or applying higher plasma RF generator power. In addition, when the temperature rise effect is reduced via application of either higher power or increased pressure, the content of nitrogen in the layer increases while the contribution of the  $\text{CH}_n$  terminal bonds decreases [26]. In another article, Jonas et al. reported formation of  $\text{Si}_x\text{N}_y(\text{H})$  and C:N:H layers by plasma-assisted chemical vapor deposition method [27]. They observed the following bands: C–N ( $1020\text{--}1280\text{ cm}^{-1}$ ), CN ( $1610\text{--}1660\text{ cm}^{-1}$ ), N–H bending ( $1590\text{ cm}^{-1}$ ),  $\text{NH}_2$  bending ( $1555\text{--}1590\text{ cm}^{-1}$ ),  $\text{CH}_n$  bending ( $1350\text{--}1450\text{ cm}^{-1}$ ), C=C ( $1300\text{--}1500\text{ cm}^{-1}$ ), C=N stretching ( $2200\text{ cm}^{-1}$ ),  $\text{CH}_n$  stretching ( $2800\text{--}3000\text{ cm}^{-1}$ ), and N–H stretching ( $3300\text{--}3500\text{ cm}^{-1}$ ). Also, with the increase of deposition time, the intensity of all absorption bands characteristics increases. They showed that for all tested samples, the roughness of the layer's surface increased with deposition process time and the fine granular structure was observed [27]. One of the main applications of DLC thin films is the hardening of lenses and optical windows in the infrared and ultraviolet wavelength regions. Therefore, the main goal of the present study is to investigate the effect of changing the nitrogen flow rate on structural and mechanical properties of the layers. The main novelty of this paper is the preparation of DLC with nitrogen as dopant for first time by direct ion beam technique. This method has some advantages relative to the other ways for preparation of DLC layer such as faster process, ability of using different gases, ability of producing solid diamond carbon layers and industrial samples.

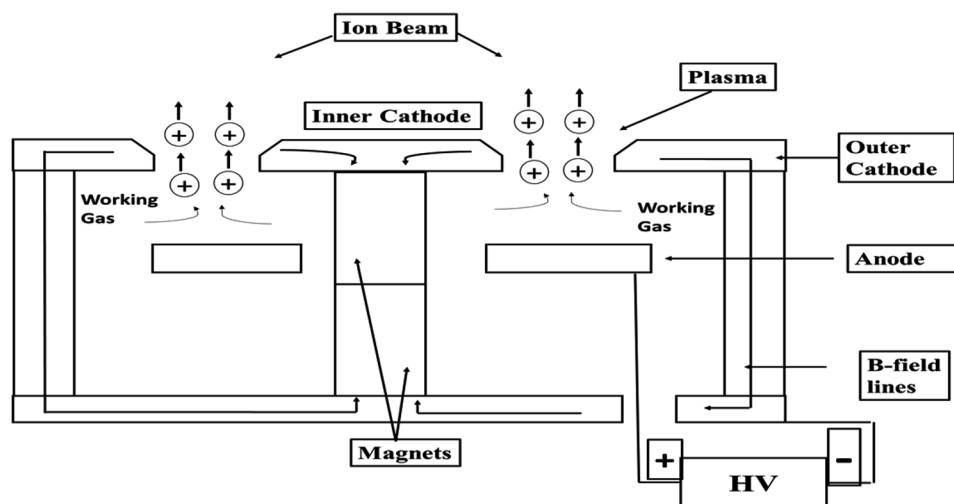
In the present investigation, N-DLC films were deposited by direct ion beam at room temperature on glass and Si substrates. The optical, structural, morphological, and mechanical properties of the prepared samples were studied. Raman analysis was used to investigate the structural properties of N-DLC samples. Morphological properties of the

N-DLC samples were studied via atomic force microscopy (AFM). By calculating the curvature of the films after deposition and using the Stoney's equation, the internal stress was measured. The nanoindentation tester was applied to investigate the mechanical properties of the DLC samples. Morphological characteristics showed reduction in film average roughness upon increasing nitrogen flow rate. Raman spectroscopic studies revealed that the amount of graphitic  $\text{sp}^2$  bonding and size of the graphite cluster increase with N doping. The N-DLC films prepared by direct ion beam deposition in this study showed good optical and mechanical properties indicating their capability of being used in optical devices. The novelty of this paper may be the finding that by increasing the amount of nitrogen content of an N-DLC film, its band gap energy, stress and roughness decreases, while its optical transmittance does not change significantly, so it can be used as a protective layer on the optical lenses.

## 2 Experimental details

N-DLC samples were prepared using anode layer system by 150 sccm methane (high purity  $> 99.999\%$ ) on the glass and Si (100) substrates with the thickness of 2.05 mm and diameter of 34.91 mm. Figure 1 shows a diagram of anode layer system as well as the working principle. The gas was introduced directly in the channel of discharge. The anode layer system was powered by a DC power supply in the voltage regulation mode. The strong magnetic field between the external and internal poles, in addition to keeping a strong electric field in the discharge plasma, led the electrons to be suspended. Glass and Si (100) substrates were cleaned in an ultrasonic bath with acetone and, then, dried by high purity  $\text{N}_2$  gas (purity 99.999%). The substrates were fixed on a static holder at an approximate distance of 15 cm from the ion source. The DLC thin films were doped by different

**Fig. 1** A schematic of anode layer source and working principle



nitrogen flow rates (5, 10, 20, 40, and 50 sccm). They were labeled as N<sub>5</sub>-DLC, N<sub>10</sub>-DLC, N<sub>20</sub>-DLC, N<sub>40</sub>-DLC, and N<sub>50</sub>-DLC, respectively. The ion source was worked at the voltage of 1.9 kV to clean plasma of the substrate in the chamber before deposition, while argon gas (purity 99.99%) was flown via the gun by the flow rate of 25 sccm. For all the processes, the pressure in the vacuum system pumped down to  $6 \times 10^{-6}$  mbar.

Surface morphology of all the N-DLC samples was investigated by AFM (Park Scientific AUTO PROBECP). Their optical properties were further examined by a UV–Vis spectrophotometric (Perkin-Elmer). The structural properties of the prepared specimens were also explored by Raman analysis (Takram P50C0R10 model: power up 0.5 to 70 mW and the excitation wavelength of 532 nm). The internal stress was calculated according to the Stoney equation from the curvature radius of the substrates measured by an optical interferometry. Finally, the mechanical features of N<sub>5</sub>-DLC and N<sub>40</sub>-DLC samples were evaluated by a nanoindentation tester (Compact Platform, Switzerland) using the continuous stiffness measurement (CSM) technique. The CSM technique is the most reliable method which has been widely used for evaluating the mechanical properties of thin films from the load–displacement curves of the indenter (CSM Instruments).

## 3 Results and discussion

### 3.1 Morphological characterization

Field emission scanning electron microscope (FESEM) was used to measure the thickness of the DLC thin films. Figure 2 represents the cross section and surface views of the DLC thin films deposited at different nitrogen flow rates (0, 5, 10, 20, 40, and 50 sccm). The thickness of DLC thin films obtained after processing by using Digimizer software [28]. The thickness of DLC, N<sub>5</sub>-DLC, N<sub>10</sub>-DLC, N<sub>20</sub>-DLC, N<sub>40</sub>-DLC, and N<sub>50</sub>-DLC samples were estimated 269, 285, 250, 274, 290, and 260 nm, respectively. The cross section images indicated that all the samples were uniform, compact with good adhesion on glass substrate, the reason for which may be attributed to the use of methane or propane as precursor of carbon [29–31]. Furthermore, good agreement was found between actual and estimated thicknesses of the samples. Comparing the surface images of the samples show that with increasing nitrogen flow rates, nanoscale particles has increased. These nanoscale particles are more specific in N<sub>10</sub>-DLC, N<sub>20</sub>-DLC, and N<sub>50</sub>-DLC samples. These results are in good agreement with the results obtained using AFM analyze.

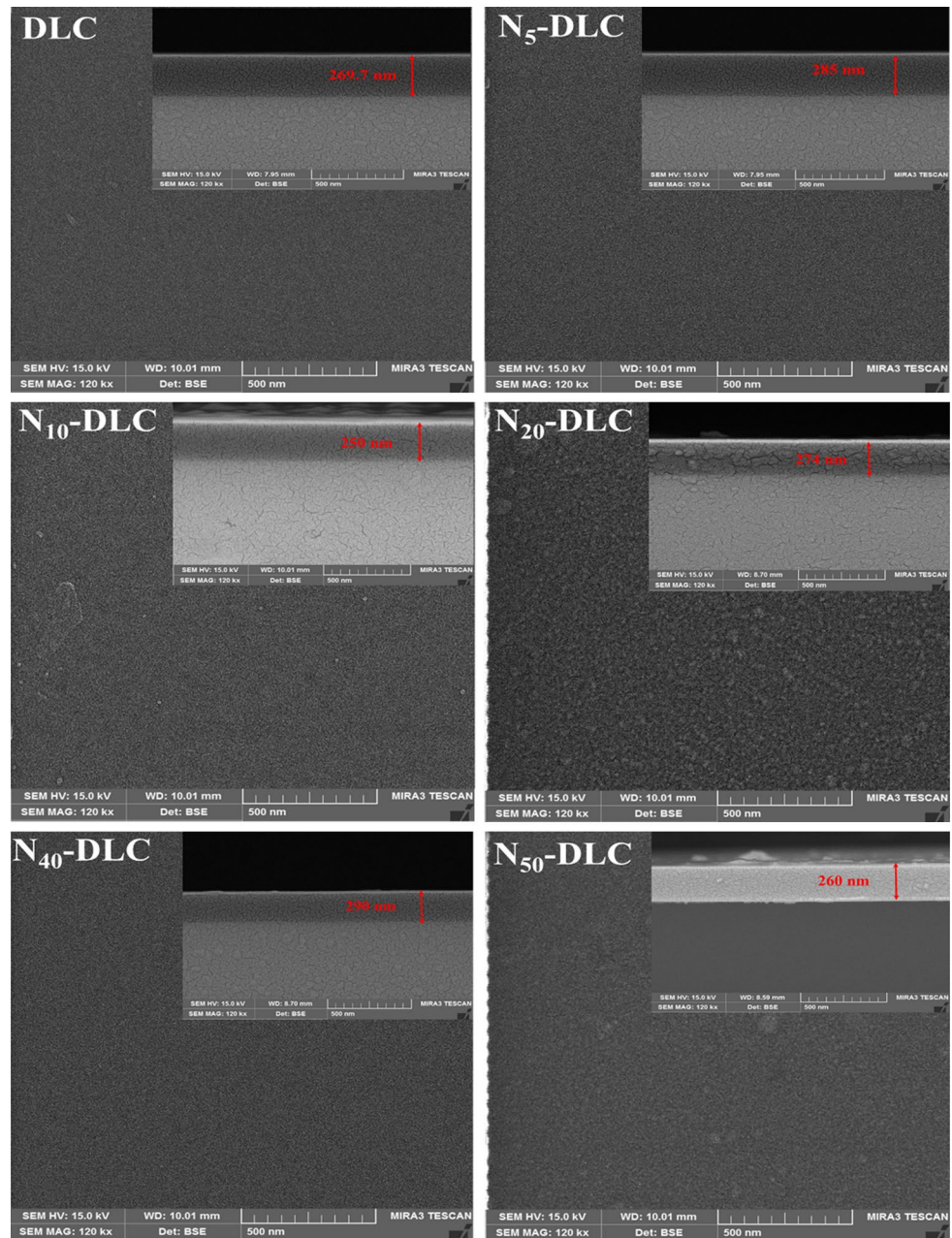
Morphological characteristics of the N-DLC samples were studied via AFM analysis. Figure 3 indicates the

3D AFM images of DLC, N<sub>5</sub>-DLC, N<sub>10</sub>-DLC, N<sub>20</sub>-DLC, N<sub>40</sub>-DLC, and N<sub>50</sub>-DLC samples. By increasing the N<sub>2</sub> content from 5 to 40 sccm, their average roughness reduced and their surface became much smoother. The average roughness ( $R_a$ ) of DLC film alone was estimated 4.3 nm. The average roughness ( $R_a$ ) as a function of N<sub>2</sub> incorporation in the DLC film is indicated in Fig. 4. With the increment of N<sub>2</sub> incorporation (from 0 to 40 sccm), the average roughness reduced (from 4.5 to 0.68 nm). Doping nitrogen into DLC films decreased their hydrogen content [32]. Generally, the surface roughness of DLC film is affected by surface motion, graphitic recrystallization, and substrate temperature [33]. In the present study, the substrate temperature was kept constant for all the samples, while graphitic recrystallization changed for different N<sub>2</sub> contents. The root-mean-square (RMS) roughness of all the N-DLC ranged from 2.7 to 1.02 nm. The RMS roughness values as a function of N<sub>2</sub> incorporation are indicated in Fig. 4. Tang et al. [34] reported RMS values of 0.35 nm for  $\alpha$ -C:H:N and 0.5–0.8 nm for  $\alpha$ -C:H samples. The RMS values depend on the deposition method and the thickness of the layers. Comparing the results, it can be found that End-Hall ion beam deposition produces smoother DLC thin films than direct ion beam method even if the films prepared in this work are much thicker. Also RMS and surface roughness increase linearly with film thickness, as reported by Logothetidis and Stergioudis [35]. Waltman et al. [36] reported RMS roughness values of 0.8 and 1.2 nm for  $\alpha$ -C:H:N and  $\alpha$ -C:H samples. All parameters for the morphological characteristics of the DLC samples are given in Table 1. The thickness of DLC samples was determined using FESEM and the values are given in Table 1.

### 3.2 Raman characterization

The DLC films bonding configuration was analyzed by Raman spectroscopy. Raman analysis is a standard tool to describe the microstructural information and the nature of carbon bonding [37]. Raman analysis of DLC films is usually composed of two peaks: D (disorder) peak around wavenumber 1370 cm<sup>-1</sup> and G (graphite) peak situated in the wavenumber range 1500–1650 cm<sup>-1</sup>. The formation of ordered sp<sup>2</sup> clusters and sp<sup>2</sup> vibrations of stretching caused by the aromatic ring, respectively [38, 39]. Raman plot of all the nitrogen doped samples is shown in Fig. 5. In this figure, two Raman peaks of 1576 cm<sup>-1</sup> and 1367 cm<sup>-1</sup> related to G and D peaks are respectively observed, indicating a typical DLC structure. Figure 6 demonstrates fitting two Gaussian peaks of N<sub>5</sub>-DLC, N<sub>20</sub>-DLC, and N<sub>40</sub>-DLC thin films. One can basically observe G peak movement to the higher values and increment in the intensity of D peak upon increasing N<sub>2</sub> gas flow rate in the figure. From fitting data, the intensity ratio of D and G peaks ( $I_D/I_G$ ), G peak position, and full

**Fig. 2** The cross section and surface views of the DLC thin films deposited at different nitrogen flow rates



width at half maximum (FWHM) of peaks can be extracted. The G peak position and FWHM of the DLC samples versus  $N_2$  gas flow rate are indicated in Fig. 7. It is observed from the figure that by increasing  $N_2$  content, G peak position moved to the higher wavenumbers. It was also observed that DLC thin films were graphitized, which could be due to the growth and formation of  $sp^2$  clusters [40]. These behaviors were attributed to the structural ordering of DLC samples [38]. Lee et al. [38] reported that the G peak position moved to the higher intensities by increasing  $N_2$  content. Tsuchiya et al. [24] prepared N-DLC films by PECVD technique and studied the effects of N content on the structural properties. They indicated that the G peak moved to the higher

wavenumbers by increasing  $N_2$  content, which could be due to the structural ordering of DLC films.

By increasing  $N_2$  content, FWHM of G peak shifted to the lower wavenumbers. As the  $sp^2$ -rich cluster size with the  $N_2$  content increased, the disorders in the DLC samples diminished and resulted in a reduction in the FWHM of G peak [18]. Polaki et al. [18] reported DLC samples deposited on Si (100) substrate with different  $N_2$  contents by PECVD technique. By increasing  $N_2$  flow rate, they indicated a structure of graphitic in DLC samples.

It is necessary to discuss about the intensity ratio of D and G peaks ( $I_D/I_G$ ) in order to describe the structure of the DLC samples. The intensity ratio  $I_D/I_G$  is a measure of the number



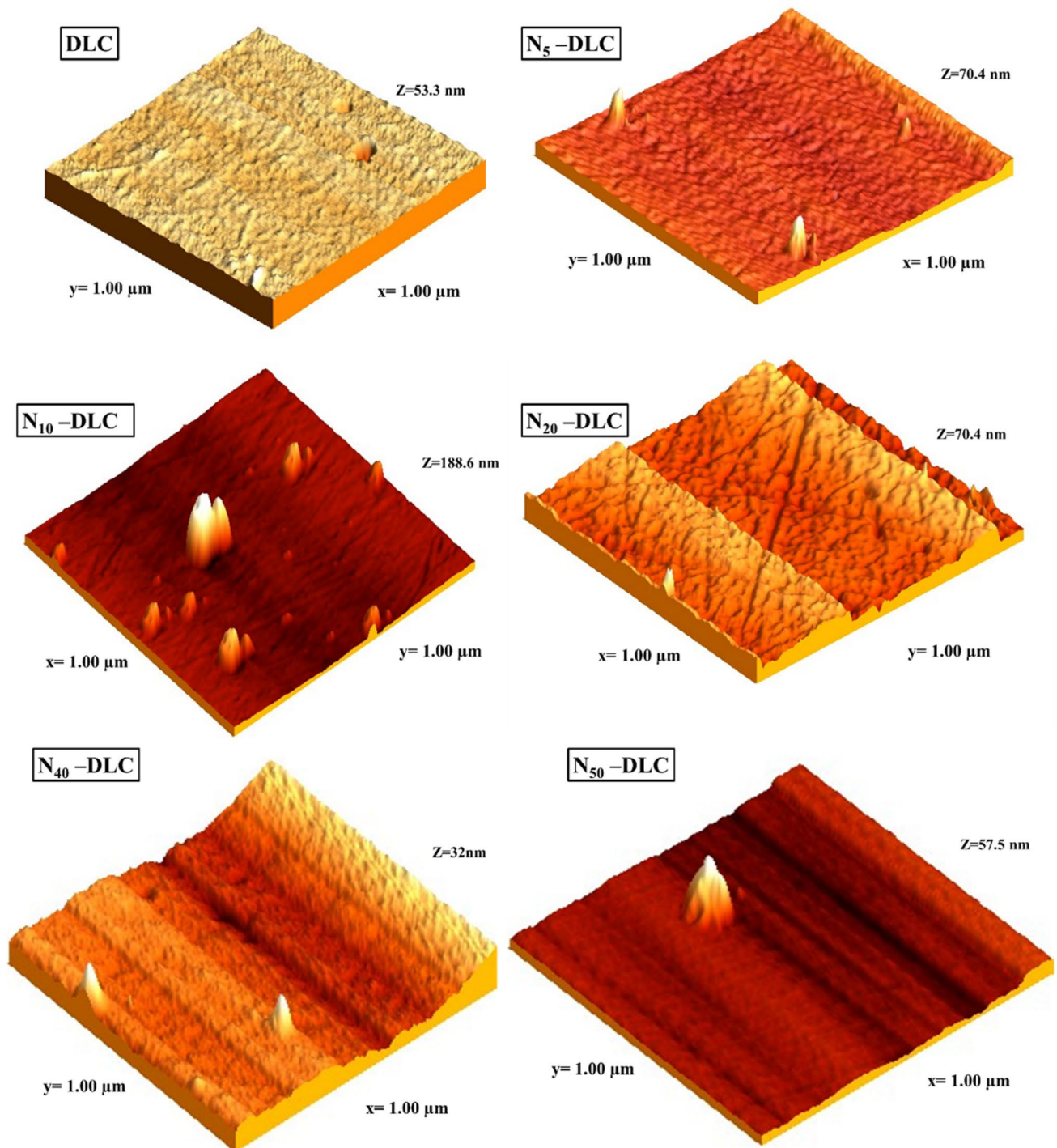


**Fig. 3** 3D AFM images of all the DLC samples

and size of  $sp^2$  clusters organized in rings. High  $I_D/I_G$  ratio of the DLC samples is an indication of increment in the  $sp^2$  clusters in aromatic rings, whereas its low ratio means the  $sp^2$  clusters are relatively organized in chains. The  $I_D/I_G$  ratio of all the N-DLC thin films versus  $N_2$  content is represented in Fig. 8. It can be observed that this ratio sharply increases by

$N_2$  content. The size of the graphite cluster ( $L_a$ ) was calculated using the Ferrari and Robertson equation [41]:

$$\frac{I_D}{I_G} = C \cdot L_a^2, \quad (1)$$

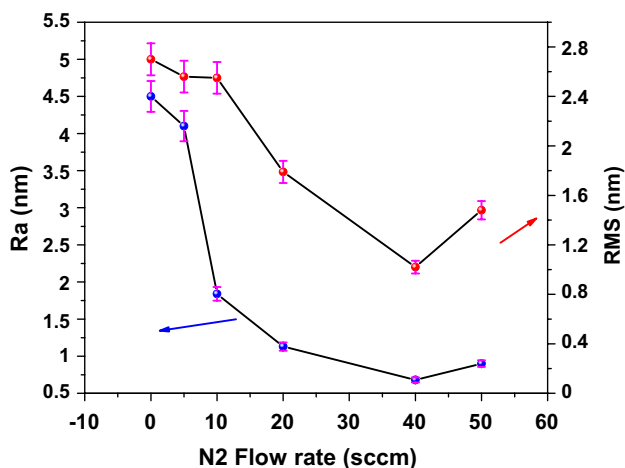


Fig. 4 The  $R_a$  values and RMS values versus of  $N_2$  flow rate

where  $C$  is  $\sim 0.0055$ .  $L_a$  values versus  $N_2$  gas flow rate for all the N-DLC samples are presented in Fig. 8. It can be seen that the size of graphite clusters increased with the  $N_2$  content. The  $I_D/I_G$  ratio also increased from 0.74 to 0.9, followed by an increment in the graphite cluster size from 1.16 to 1.28 Å. All the parameters regarding the structure of the DLC samples are given in Table 1.

### 3.3 FTIR measurement

FTIR plot of all the N-DLC samples on Si substrates in the range  $1400\text{--}3500\text{ cm}^{-1}$  is presented in Fig. 9. In this figure, a few peaks belonging to the FTIR characteristics of DLC film doped with  $N_2$  gas, are observed. The figure indicates a broad peak in FTIR pattern of all the samples at  $2910\text{ cm}^{-1}$  due to C–H stretching vibrations mode. A reduction in the intensity of the C–H bond by increasing the  $N_2$  doped is observed, showing low hydrogen incorporation in the  $N_{50}$ -DLC samples. Another group of intense absorption band at around  $2400\text{ cm}^{-1}$  is attributed to C–O bonds. An additional group of intensive absorption band observed at around  $2420\text{ cm}^{-1}$  is relevant to C–O [41, 42]. The intense absorption band centered at  $1450\text{ cm}^{-1}$  is identified as the stretching vibration of C=C bond, which is in agreement with the reported result [43]. Considering Fig. 9,

three peaks including C–N,  $C\equiv N$ , and N–H mods appeared at  $1740\text{ cm}^{-1}$ ,  $2330\text{ cm}^{-1}$ , and  $3360\text{ cm}^{-1}$ , respectively. Our analysis of FTIR data matches with the results reported by others [44, 45]. The research conducted by Kaufman et al. [44] shows two lines active in the  $sp^2$  area at around  $1550$  and  $1375\text{ cm}^{-1}$ . By increasing  $N_2$  incorporation, a weaker doublet was indicated at  $2110\text{--}2210\text{ cm}^{-1}$  in the  $sp$  area [44]. The  $2850$  and  $2958\text{ cm}^{-1}$  peaks are assigned to the symmetric modes of  $sp^3\text{-CH}_3$  and  $sp^3\text{-CH}_2$  groups, respectively [45].

### 3.4 UV–Vis analyzes

The transmittance and reflection of N-DLC samples prepared at different  $N_2$  flow rates is demonstrated in Fig. 10. The average optical transmittance of  $N_5$ -DLC,  $N_{10}$ -DLC,  $N_{20}$ -DLC,  $N_{40}$ -DLC, and  $N_{50}$ -DLC samples in the  $400\text{--}2200\text{ nm}$  wavelength region was calculated as 67.88, 66.67, 61.09, 57.70, and 61.87%, respectively. This result indicates that the optical transmittance of N-DLC films diminished by increasing the  $N_2$  flow rate. This finding is evidence of the microstructure changes in the samples as the result of increasing the  $N_2$  content. This reduction in optical transmittance is probably related to the growth of the  $sp^2$  fraction.

The absorption coefficient ( $\alpha$ ) has been measured by the following equation [46] to get the optical band gap ( $E_g$ ) of N-DLC samples:

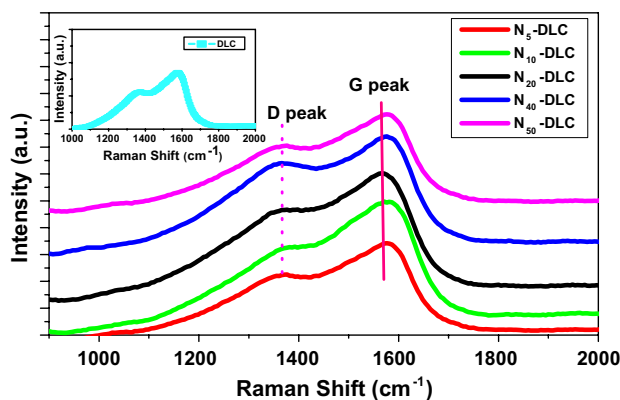


Fig. 5 Raman plot of all the nitrogen doped DLC samples

**Table 1** Optical, structural, mechanical, and morphological parameters of  $N_2$ -DLC samples at various  $N_2$  contents

Sample	$R_a$ (nm)	RMS (nm)	$I_D/I_G$	$L_a$ (Å)	Band gap (eV)	Thickness (nm)
DLC	$4.5 \pm 0.21$	$2.7 \pm 12$	0.74	1.14	$2.87 \pm 0.7$	269
$N_5$ -DLC	$4.10 \pm 0.2$	$2.56 \pm 0.12$	0.75	1.16	$2.61 \pm 0.06$	285
$N_{20}$ -DLC	$1.84 \pm 0.1$	$2.55 \pm 0.13$	0.76	1.17	$2.54 \pm 0.05$	250
$N_{40}$ -DLC	$1.13 \pm 0.06$	$1.79 \pm 0.09$	0.83	1.23	$2.48 \pm 0.04$	274
$N_{50}$ -DLC	$0.68 \pm 0.03$	$1.02 \pm 0.05$	0.89	1.27	$2.27 \pm 0.03$	290
$N_5$ -DLC	$0.90 \pm 0.04$	$1.48 \pm 0.07$	0.9	1.28	$2.39 \pm 0.04$	260

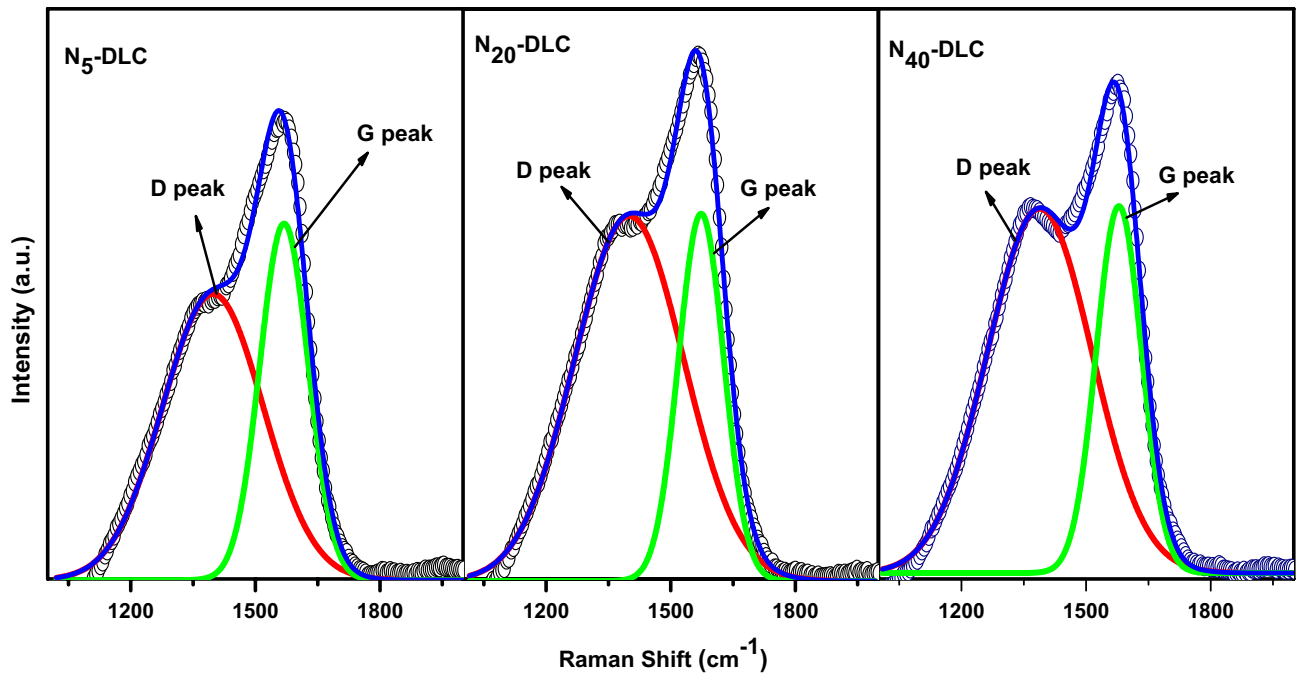


Fig. 6 Fitted two Gaussian peaks for N<sub>5</sub>-DLC, N<sub>20</sub>-DLC, and N<sub>40</sub>-DLC thin films

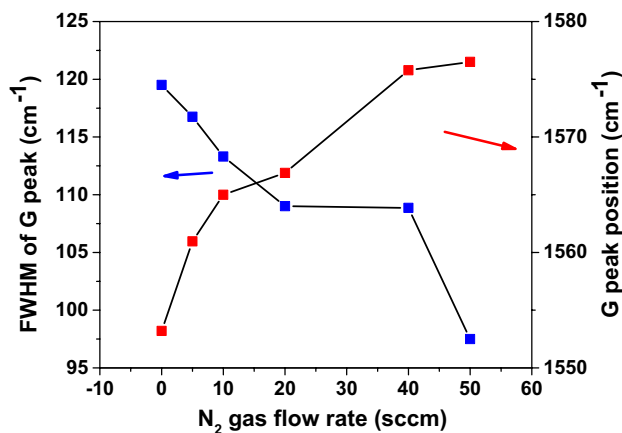


Fig. 7 G peak position and FWHM of all DLC samples

$$\alpha = \frac{1}{d} \ln \frac{(1 - R)^2}{T}, \tag{2}$$

where T is the transmission, R is the reflection, and d is the thickness of the films. The optical band gap of the samples has been calculated using Tauc equation [47]:

$$(\alpha h\nu)^{1/2} = A(h\nu - E_g), \tag{3}$$

where h is the Planck's constant, A depends on the effective masses of holes and electrons and is constant, and n is a constant equal to 0.5 for direct band gap as well as 2 for

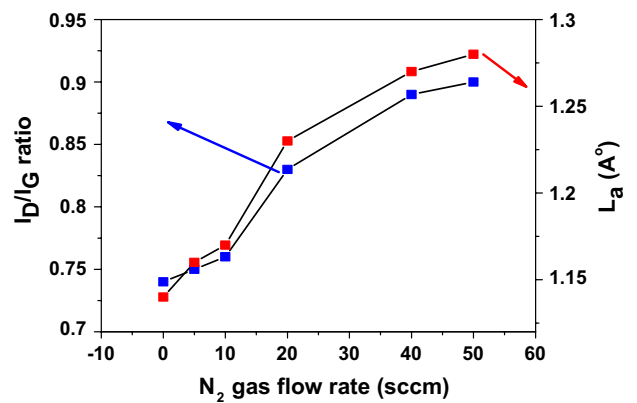


Fig. 8 The I<sub>D</sub>/I<sub>G</sub> ratio and L<sub>a</sub> of all the nitrogen doped DLC samples

an indirect optical band gap. Figure 11 shows the plot of  $(\alpha h\nu)^{1/2}$  as a function energy of photons ( $h\nu$ ) in N-DLC samples prepared at various N<sub>2</sub> flow rates. The band gap energy values are obtained by extrapolating the linear portion of the curves to x axis. The results are presented in Table 1. The estimated optical band gaps for the DLC, N<sub>5</sub>-DLC, N<sub>10</sub>-DLC, N<sub>20</sub>-DLC, N<sub>40</sub>-DLC, and N<sub>50</sub>-DLC samples were 2.87, 2.74, 2.48, 2.38, 2.2, and 2.29 eV, respectively. This results shows that when the N<sub>2</sub> flow ratio was increased the optical bandgap decreased. Rodil and Muhl [48] showed that the bandgap of tetrahedral carbon nitride films decreased sharply with increasing N/C ratio and the opposite trend was observed for amorphous carbon nitride films. Tsuchiya

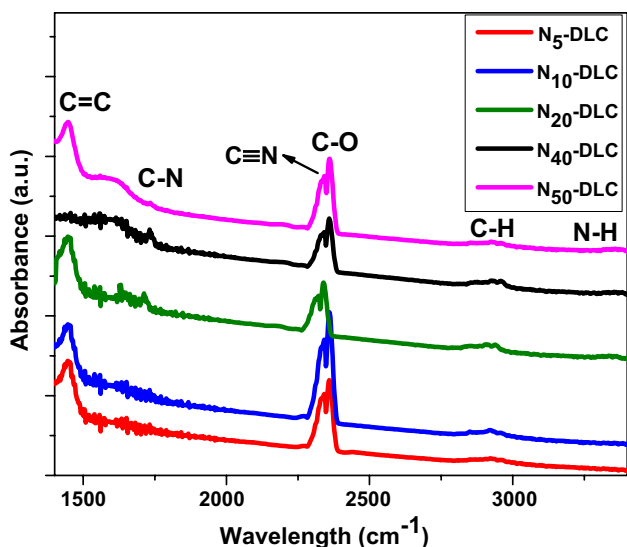


Fig. 9 FTIR plot for all the nitrogen doped DLC samples in the range 1400–3500 cm<sup>-1</sup>

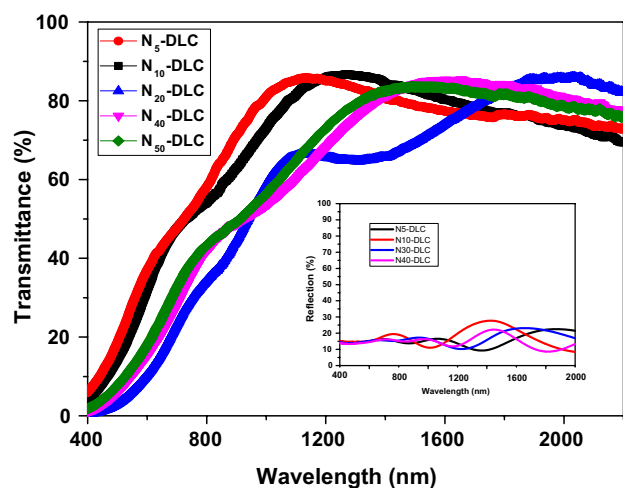


Fig. 10 The transmittance of N-DLC samples with various N<sub>2</sub> flow rate in the UV–Vis–NIR area

et al. [24] showed that when the N<sub>2</sub> flow ratio was increased from 0 to 10%, the optical bandgap decreased from 1.16 to 1.06 eV. Zkria et al. [49] showed that the indirect optical bandgap decreases from 1.7 to 1.28 eV by nitrogen doping. Seker et al. [50] reported the optical band gap for N-DLC samples in the range of 1.92 to 2.29 eV. Also, they reported that the optical band gap decreased upon increasing N<sub>2</sub> contents. It is clear that N<sub>2</sub> contents favored the increase of sp<sup>2</sup> clusters in size and number [21], which was consistent with the results of Raman studies already provided. Considering the results, the increase in the disordering and size of sp<sup>2</sup> clusters would affect the optical properties of N-DLC samples. The band gap of DLC samples was not only

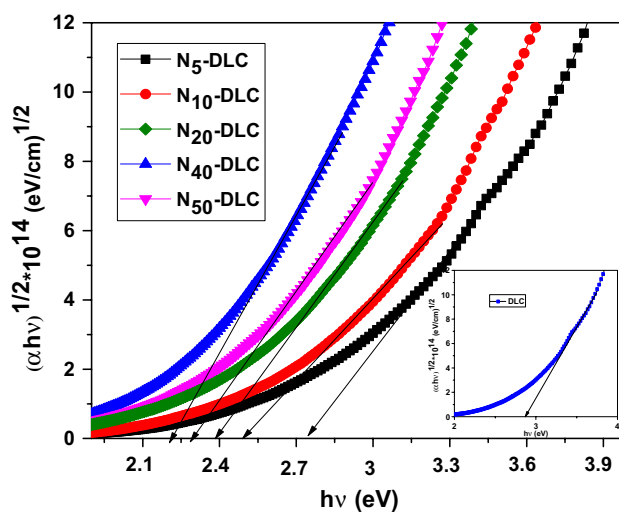


Fig. 11 The curve of  $(\alpha hv)^{1/2}$  as a function  $h\nu$  of N-DLC samples with various N<sub>2</sub> flow rates

proportional to the sp<sup>3</sup> sites but controlled using distortions and ordering of π states in sp<sup>2</sup> phases [51, 52]. The π state of sp<sup>2</sup> phases was near the Fermi level conduction and valence band edges. The reduction in the energy gap sourced from the π/π\* transfer occurred in the sp<sup>2</sup> domain [53].

### 3.5 Evaluation of internal stress

To calculate the internal stress of all the samples, slide glass substrate (34.91 mm in diameter and 2.05 mm in thickness) was selected. The internal stress was measured by calculating the film curvature after deposition on one side of the substrate via the Stoney’s relation [54]:

$$\sigma = \frac{E_s}{6(1 - \nu_s)} \left( \frac{t_s^2}{t_f} \right) \left( \frac{1}{R_2} - \frac{1}{R_1} \right), \tag{4}$$

where  $\sigma$  is the internal stress,  $\nu_s$  is the substrate Poisson’s ratio,  $E_s$  is the substrate Young modulus,  $R_1$  and  $R_2$  are the substrate curvatures before and after deposition,  $t_s$  and  $t_f$  are the thicknesses of substrate and film, respectively. The values adopted for the glass substrate constants ( $\nu_s = 0.22$ ,  $E_s = 1.03 \times 10^{10} \text{ Nm}^{-2}$ ) were taken from Zou et al. [55]. The internal stress of N-DLC samples was calculated by the stress induced from the interferometric surface profiler. The radius ( $R$ ) of the substrates before and after the deposition was calculated using the observation of Newton’s rings method by the optical interferometry. The radius of the substrate curvature was determined using the following equation:

$$R = \frac{d_m^2}{4m\lambda} \quad (m = 1, 2, 3, \dots), \tag{5}$$



where  $d_m$  is the  $m$ th dark interference fringe diameter and  $\lambda$  is the wavelength of the light ( $\lambda = 589.3$  nm). Figure 12 indicates the internal stress of N-DLC samples versus  $N_2$  content. It was observed that, with the  $N_2$  content increase, the internal stress declined. By increasing the  $N_2$  content from 0 to 40 sccm, the internal stress reduced from 1.9 to 0.58 GPa. For the  $N_{50}$ -DLC sample, the internal stress was measured as 1.4 GPa. Sharifahmadian et al. reported the same results for N-DLC thin films [56]. The three important factors causing the reduction in internal stress are increment of the  $sp^2$ -C bonds [57], increase of the induced ad-atom mobility [58], and distortion of the bond angle [58]. Raman analysis confirmed that incorporating  $N_2$  into DLC films increased the values of  $sp^2$  hybridized atoms. In addition, the incorporation of  $N_2$  decreased the coordination numbers of the films, which in turn declined the degree of over-constraining in the N-DLC samples; hence decreasing the stress [59]. Furthermore, by the  $N_2$  incorporation,  $C\equiv N$  bonds were formed, leading to a weaker network between the  $sp^2$  clusters in the N-DLC films, also reducing the internal stress in the films [60]. As illustrated in Fig. 12, the internal stress of  $N_{50}$ -DLC was higher than that of  $N_{40}$ -DLC sample. The higher internal stress of the  $N_{50}$ -DLC film might be due to the organization of a larger amount of  $N_2$  plasma during its deposition process [21].

### 3.6 Mechanical properties

Finally, nanoindentation measurements were done on  $N_5$ -DLC and  $N_{40}$ -DLC samples to investigate their mechanical properties. Hardness (H), elastic modulus (E), plasticity (H/E), residual displacement after load removal with displacement at the most load ( $h_{res}/h_{max}$ ), and elastic recovery (%ER) were performed following Oliver and Pharr's model

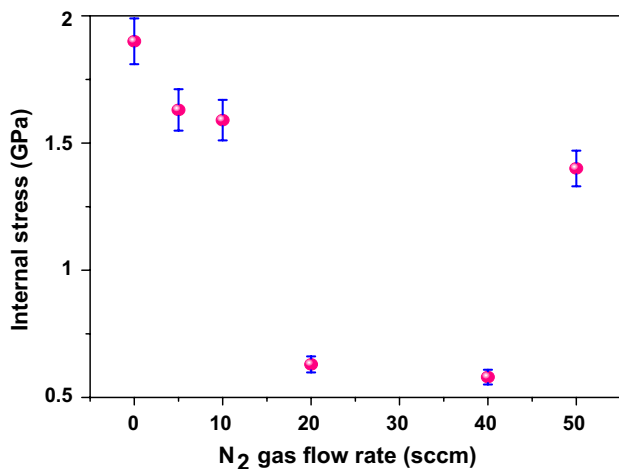


**Fig. 12** The internal mechanical stress of N-DLC samples versus  $N_2$  content

[61]. The maximum depth in the nanoindentation test was limited to lesser than one-tenth of the thickness of the DLC sample. The load versus displacement plot for  $N_5$ -DLC and  $N_{20}$ -DLC samples is shown in Fig. 13. The results of H and E for these samples are indicated in Table 2. Mechanical hardness was measured from 5 points of the sample surface and the values given in Table 2 are the average mechanical hardness. According to the results, high hardness and elastic modulus were obtained for the samples. It was found that with increasing N content from 5 to 40 sccm, hardness was declined from 26.4 to 22.6 GPa, in addition, elastic modulus was decreased from 107.9 to 104.3 GPa. It may be mentioned that E and H of DLC samples depend on the  $sp^3$  bonding fraction [62].  $\pi$  Bonds of  $sp^2$  bonding structures lead to the reduction of the mechanical properties and  $sp^3$  bonding is combined with a covalent bond to improve the mechanical properties. According to the Raman's analysis,  $sp^2$  bands increases by the increase of nitrogen content; thus, it may be the reason for a decline in the hardening and the elastic modulus of the samples. This observation was very similar to those reported by others [63, 64].

The plasticity index parameter (H/E) is the main parameter in explaining the wear resistance properties of films due to combined effect [65]. The H/E values for  $N_5$ -DLC and  $N_{40}$ -DLC films are presented in Table 2. The results show that by increasing nitrogen content, the H/E decreased from 0.244 to 0.216, because the graphite-like  $sp^2$  bonding formation started. The %ER is the main parameter for

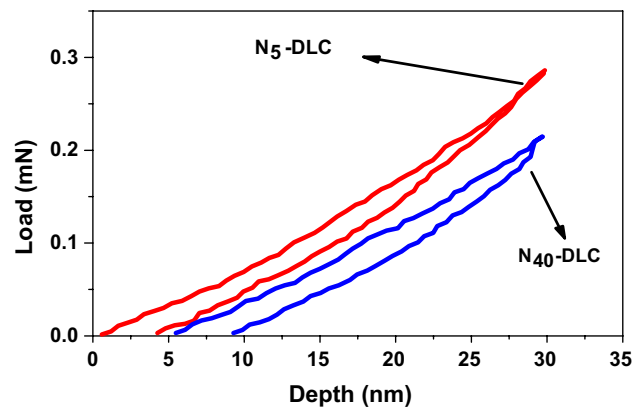


**Fig. 13** Load–displacement curves of the  $N_5$ -DLC and  $N_{40}$ -DLC samples

**Table 2** Values of H, E, %ER, H/E, and  $h_{res}/h_{max}$  for  $N_5$ -DLC and  $N_{40}$ -DLC films

Samples	H (GPa)	E (GPa)	%ER	H/E	$h_{res}/h_{max}$
$N_5$ -DLC	$26.4 \pm 1.3$	$107.9 \pm 5.4$	86	0.244	0.14
$N_{40}$ -DLC	$22.6 \pm 1.1$	$104.3 \pm 5.2$	69	0.216	0.31

hard coatings. Higher the %ER factor value higher be the hardness value of the films and more useful the coatings for the tribological applications [65]. The values of %ER were measured with the following equation [66]:

$$\%ER = \frac{h_{\max} - h_{\text{res}}}{h_{\max}} \times 100. \quad (6)$$

As can be seen in Table 2, %ER increased from about 69% to 86% by increasing N incorporation from 5 to 40 sccm. The results of %ER are in good agreement with the similar results for H. Finally, the  $h_{\text{res}}/h_{\max}$  parameter provided information analogous to that of ER with a variable domain of validity. The values of  $h_{\text{res}}/h_{\max}$  for N<sub>5</sub>-DLC and N<sub>40</sub>-DLC samples are presented in Table 2. Referring to Table 2, the values %ER decreased from 69 to 86% by increasing N content from 5 to 40 sccm. It was also found that the  $h_{\text{res}}/h_{\max}$  values were in the line with H, E, and H/E results.

## 4 Conclusions

N-DLC films were prepared by direct ion beam deposition technique (at room temperature) on Si and glass substrates to study the effects of N doping on their structural, optical, and mechanical properties. Morphological characteristics showed a reduction in average film roughness (from 4.1 to 0.68 nm) upon increasing nitrogen flow rate (from 5 to 40 sccm). Raman studies revealed that the number of graphitic sp<sup>2</sup> bonding and the size of the graphite clusters increased from 1.16 to 1.27 Å with N doping. With increasing nitrogen flow rate (from 5 to 40 sccm) the energy gap decreased from 2.61 to 2.27 eV and the internal stress of the deposited samples decreased from 1.63 to 0.58 GPa. The mechanical features of the DLC films show that with increasing N incorporation from 5 to 40 sccm, hardness declined from 26.4 to 22.6 GPa, elastic modulus also decreased from 107.9 to 104.3 GPa. Therefore, in this study, the N-DLC samples prepared by direct ion beam deposition technique showed good optical and mechanical properties; indicating the possibility of using them in optical devices.

## References

- X. Yan, T. Xu, G. Chen, S. Yang, H. Liu, Study of structure, tribological properties and growth mechanism of DLC and nitrogen-doped DLC films deposited by electrochemical technique. *Appl. Surf. Sci.* **236**, 328–335 (2004)
- Z. Han, H. Li, G. Lin, C. Dong, Influence of nitrogen flow rate on the microstructure and properties of N and Me (Me=Cr, Zr) co-doped diamond-like carbon films. *J. Mater. Sci. Technol.* **26**, 967–972 (2010)
- L. Ru, J. Huang, L. Gao, B. Qi, Hydrogen-free diamond-like carbon films prepared by microwave electron cyclotron resonance plasma-enhanced direct current magnetron sputtering. *Thin Solid Films* **519**, 86–90 (2010)
- R. Zarei Moghadam, M.H. Ehsani, H. Rezagholipour Dizaji, P. Kameli, M. Jannesari, Modification of hydrophobicity properties of diamond like carbon films using glancing angle deposition method. *Mater. Lett.* **220**, 301–304 (2018)
- R. Zarei Moghadam, H. Rezagholipour Dizaji, M.H. Ehsani, P. Kameli, M. Jannesari, Correlation study of structural, optical, and hydrophobicity properties of diamond-like carbon films prepared by an anode layer source. *Mater. Res. Express* **6**, 055601 (2019)
- E. Ali, Ch. Donnet, Tribology of diamond-like carbon films: recent progress and future prospects. *J. Phys. D* **39**, 311 (2006)
- J.D. Beard, S. Aleksandrov, C.H. Walker, D. Wolverson, J.M. Mitchels, S.N. Gordeev, Magnetically enhanced plasma coating of nanostructures with ultrathin diamond-like carbon films. *RSC Adv.* **4**, 26635–26644 (2014)
- M.K. Kuntumalla, V.V.S.S. Srikanth, S. Ravulapalli, U. Gangadharini, H. Ojha, N.R. Desai, C. Bansal, SERS activity of Ag decorated nanodiamond and nano-β-SiC, diamond-like-carbon and thermally annealed diamond thin film surfaces. *Phys. Chem. Chem. Phys.* **17**, 21331–21336 (2015)
- J.K. Luo, Y.Q. Fu, H.R. Le, J.A. Williams, S.M. Spearing, W.I. Milne, Diamond and diamond-like carbon MEMS. *J. Micromech. Microeng.* **17**, 147 (2007)
- D.S. Grierson, R.W. Carpick, Nanotribology of carbon-based materials. *Nano Today* **2**, 12–21 (2007)
- Z. Seker, H. Ozdamar, M. Esen, R. Esen, H. Kavak, The effect of nitrogen incorporation in DLC films deposited by ECR microwave plasma CVD. *Appl. Surf. Sci.* **314**, 46–51 (2014)
- K. Zhou, P. Ke, X. Li, Y. Zou, A. Wang, Microstructure and electrochemical properties of nitrogen-doped DLC films deposited by PECVD technique. *Appl. Surf. Sci.* **329**, 281–286 (2015)
- S.F. Ahmed, M.W. Moon, K.R. Lee, Effect of silver doping on optical property of diamond like carbon films. *Thin Solid Films* **517**, 4035–4038 (2009)
- M. Ikeyama, S. Nakao, Y. Miyagawa, S. Miyagawa, Effects of Si content in DLC films on their friction and wear properties. *Surf. Coat. Technol.* **191**, 38–42 (2005)
- P. Safaie, A. Eshaghi, S.R. Bakhshi, Optical properties of oxygen doped diamond-like carbon thin films. *J. Alloys Compd.* **672**, 426–432 (2016)
- N. Fujisawa, T.F. Zhang, O.L. Li, K.H. Kim, Substrate-independent stress–strain behavior of diamond-like carbon thin films by nanoindentation with a spherical tip. *J. Mater. Sci.* **33**, 699–708 (2018)
- C. Donnet, A. Erdemir (eds.), *Tribology of diamond-like carbon films: fundamentals and applications* (Springer, Heidelberg, 2008), pp. 318–319
- S.R. Polaki, K. Ganesan, S.K. Srivastava, M. Kamruddin, A.K. Tyagi, The role of substrate bias and nitrogen doping on the structural evolution and local elastic modulus of diamond-like carbon films. *J. Phys. D* **50**, 175601 (2017)
- G.A. Viana, E.F. Motta, M.E.H.M. Da Costa, F.L. Freire Jr., F. das Chagas Marques, Diamond-like carbon deposited by plasma technique as a function of methane flow rate. *Diam. Relat. Mater.* **19**, 756–759 (2010)
- D. Caschera, P. Cossari, F. Federici, S. Kaciulis, A. Mezzi, G. Padeletti, D.M. Trucchi, Influence of PECVD parameters on the properties of diamond-like carbon films. *Thin Solid Films* **519**, 4087–4091 (2011)
- D. Bootkul, B. Supsermpol, N. Saenphinit, C. Aramwit, S. Intarasiri, Nitrogen doping for adhesion improvement of DLC film deposited on Si substrate by filtered cathodic vacuum arc (FCVA) technique. *Appl. Surf. Sci.* **310**, 284–292 (2014)
- H. Li, M. Fang, Y. Hou, R. Tang, Y. Yang, C. Zhong, Q. Li, Z. Li, The different effect of the additional electron withdrawing

- cyano group in different conjugation bridge: the adjusted molecular energy levels and largely improved photovoltaic performance. *ACS Appl. Mater. Interfaces* **8**, 12134–12140 (2016)
23. V. Kopustinskias, Š. Meškinius, V. Grigaliūnas, S. Tamulevičius, M. Pucėta, G. Niaura, R. Tomašiūnas, Ion beam synthesis of  $\alpha$ -CN<sub>x</sub>:H films. *Surf. Coat. Technol.* **180**, 151–152 (2002)
  24. M. Tsuchiya, K. Murakami, K. Magara, K. Nakamura, H. Ohashi, K. Tokuda, T. Takami, H. Ogasawara, Y. Enta, Y. Suzuki, S. Ando, Structural and electrical properties and current–voltage characteristics of nitrogen-doped diamond-like carbon films on Si substrates by plasma-enhanced chemical vapor deposition. *Jpn. J. Appl. Phys.* **55**, 065502 (2016)
  25. J. Lee, B.H. Choi, J.H. Yun, Y.S. Park, Characteristics of nitrogen doped diamond-like carbon films prepared by unbalanced magnetron sputtering for electronic devices. *J. Nanosci. Nanotechnol.* **16**, 4893–4896 (2016)
  26. S. Jonas et al., Formation of six Ny(H) and C:N:H layers by plasma-assisted chemical vapor deposition method. *Thin Solid Films* **600**, 162–168 (2016)
  27. S. Jonas et al., Stability of a-C:N:H layers deposited by RF plasma enhanced CVD. *Solid State Phenom.* **147**, 738–743 (2009)
  28. M.R. Sazideh, H.R. Dizaji, M.H. Ehsani, R.Z. Moghadam, Modification of the morphology and optical properties of SnS films using glancing angle deposition technique. *Appl. Surf. Sci.* **405**, 514–520 (2017)
  29. W. Dai, A. Wang, Deposition and properties of Al-containing diamond-like carbon films by a hybrid ion beam sources. *J. Alloys Compd.* **509**, 4626–4631 (2011)
  30. Y. Wu, J. Chen, H. Li, L. Ji, Y. Ye, H. Zhou, Preparation and properties of Ag/DLC nanocomposite films fabricated by unbalanced magnetron sputtering. *Appl. Surf. Sci.* **284**, 165–170 (2013)
  31. J. Jianlg, H. Huang, Q. Wang, W. Zhu, J. Hao, W. Liu, Comparative study on structure and properties of titanium/silicon mono- and co-doped amorphous carbon films deposited by mid-frequency magnetron sputtering. *Surf. Interface Anal.* **46**, 139–144 (2014)
  32. R. Hauert, A review of modified DLC coatings for biological applications. *Diam. Relat. Mater.* **12**, 583–589 (2003)
  33. M. Constantinou, M. Pervolaraki, P. Nikolaou, C. Prouskas, P. Patsalas, P. Kelires, J. Giapintzakis, G. Constantinides, Microstructure and nanomechanical properties of pulsed excimer laser deposited DLC:Ag films: enhanced nanotribological response. *Surf. Coat. Technol.* **309**, 320–330 (2017)
  34. Y. Tang, Y.S. Li, Q. Yang, A. Hirose, Characterization of hydrogenated amorphous carbon thin films by End-Hall ion beam deposition. *Appl. Surf. Sci.* **257**, 4699–4705 (2011)
  35. S. Logothetidis, G. Stergioudis, Studies of density and surface roughness of ultrathin amorphous carbon films with regards to thickness with X-ray reflectometry and spectroscopic ellipsometry. *Appl. Phys. Lett.* **71**, 2463–2465 (1997)
  36. R.J. Waltman, H. Zhang, A. Khurshudov, D. Pocker, M.A. Karplus, B. York, Q.F. Xiao, H. Zadoori, J.U. Thiele, G.W. Tyndall, The effect of carbon overcoat thickness on the Zdol boundary lubricant film. *Tribol. Lett.* **12**, 51–60 (2002)
  37. L. Caçado, A. Jorio, M. Pimenta, Measuring the absolute Raman cross section of nanographites as a function of laser energy and crystallite size. *Phys. Rev. B* **76**, 064304–064307 (2007)
  38. A. Ferrari, J. Robertson, Interpretation of Raman spectra of disordered and amorphous carbon. *Phys. Rev. B* **61**, 14095–14107 (2000)
  39. M. Pandey, D. Bhattacharyya, D.S. Patil, K. Ramachandran, N. Venkatramani, A.K. Dua, Structural and optical properties of diamond like carbon films. *J. Alloys Compd.* **386**, 296–302 (2005)
  40. M. Chhowalla, A. Ferrari, J. Robertson, G. Amaratunga, Evolution of sp<sup>2</sup> bonding with deposition temperature in tetrahedral amorphous carbon studied by Raman spectroscopy. *Appl. Phys. Lett.* **76**, 1419–1421 (2000)
  41. A. Ferrari, J. Robertson, Resonant Raman spectroscopy of disordered, amorphous, and diamond-like carbon. *Phys. Rev. B* **64**, 075414–075427 (2001)
  42. B. Dischler, A. Bubenzer, P. Koidl, Hard carbon coatings with low optical absorption. *Appl. Phys. Lett.* **42**, 636–638 (1983)
  43. H. Nakazawa, S. Miura, R. Kamata, S. Okuno, M. Suemitsu, T. Abe, Effects of pulse bias on structure and properties of silicon/nitrogen-incorporated diamond-like carbon films prepared by plasma-enhanced chemical vapor deposition. *Appl. Surf. Sci.* **264**, 625–632 (2013)
  44. J.H. Kaufman, S. Metin, D.D. Saperstein, Symmetry breaking in nitrogen-doped amorphous carbon: infrared observation of the Raman-active G and D bands. *Phys. Rev. B* **39**, 13053 (1989)
  45. S. Kundoo, P. Saha, K.K. Chattopadhyay, Electron field emission from nitrogen and sulfur-doped diamond-like carbon films deposited by simple electrochemical route. *Mater. Lett.* **58**, 3920–3924 (2004)
  46. N. Tajik, M.H. Ehsani, R. Zarei Moghadam, H. Rezagholipour Dizaji, Effect of GLAD technique on optical properties of ZnS multilayer antireflection coatings. *Mater. Res. Bull.* **100**, 265–274 (2017)
  47. M.H. Ehsani, R. Zarei Moghadam, H. Rezagholipour Dizaji, P. Kameli, Surface modification of ZnS films by applying an external magnetic field in vacuum chamber. *Mater. Res. Express* **4**, 096408 (2017)
  48. S.E. Rodil, S. Muhl, Bonding in amorphous carbon nitride. *Diam. Relat. Mater.* **13**, 1521–1531 (2004)
  49. A. Zkria, Y. Katamune, T. Yoshitake, Effects of nitrogen doping on the electrical conductivity and optical absorption of ultranano-crystalline diamond/hydrogenated amorphous carbon films prepared by coaxial arc plasma deposition. *Jpn. J. Appl. Phys.* **55**, 07LE01-4 (2016)
  50. Z. Seker, H. Ozdamar, M. Esen, R. Esen, H. Kavak, The effect of nitrogen incorporation in DLC films deposited by ECR microwave plasma CVD. *Appl. Surf. Sci.* **314**, 46–51 (2013)
  51. Z. Zhai, H. Shen, J. Chen, X. Li, Effect of deposition pressure on the properties of amorphous carbon films by hot-filament chemical vapor deposition. *J. Mater. Sci. Mater. Electron.* **30**, 1–7 (2019)
  52. A. Hu, I. Alkhesho, H. Zhou, W.W. Duley, Optical and microstructural properties of diamond-like carbon films grown by pulsed laser deposition. *Diam. Relat. Mater.* **16**, 149–154 (2007)
  53. N. Dwivedi, S. Kumar, G.H.K. Malik, C.M.S. Rauthan, O.S. Panwar, Correlation of sp<sup>3</sup> and sp<sup>2</sup> fraction of carbon with electrical, optical and nano-mechanical properties of argon-diluted diamond-like carbon films. *J. Vac. Sci. Technol. A* **257**, 6804–6810 (2011)
  54. M.H. Fang, P.Y. Tian, M.D. Zhu, H.J. Qi, T. Fei, J.P. Lv, H.P. Liu, Laser-induced damage threshold in HfO<sub>2</sub>/SiO<sub>2</sub> multilayer films irradiated by  $\beta$ -ray. *Chin. Phys. B* **28**, 024215 (2019)
  55. J.W. Zou, K. Reichelt, K. Schmidt, B. Dischler, The deposition and study of hard carbon films. *J. Appl. Phys.* **65**, 3914–3918 (1989)
  56. O. Sharifahmadian, F. Mahboubi, S. Yazdani, Comparison between corrosion behaviour of DLC and N-DLC coatings deposited by DC-pulsed PACVD technique. *Diam. Relat. Mater.* **95**, 60–70 (2019)
  57. Y.B. Zhang, S.P. Lau, D. Sheeja, B.K. Tay, Study of mechanical properties and stress of tetrahedral amorphous carbon films prepared by pulse biasing. *Surf. Coat. Technol.* **195**, 338–343 (2005)
  58. Y.N. Kok, P.E. Hovsepian, Q. Luo, D.B. Lewis, J.G. Wen, I. Petrov, Influence of the bias voltage on the structure and the tribological performance of nanoscale multilayer C/Cr PVD coatings. *Thin Solid Films* **475**, 219–226 (2005)
  59. T. Chen, X. Wu, Z. Ge, J. Ruan, B. Lv, J. Zhang, Achieving low friction and wear under various humidity conditions by co-doping

- nitrogen and silicon into diamond-like carbon films. *Thin Solid Films* **638**, 375–382 (2017)
60. D.-J. Jan, C.-F. Ai, C.-C. Lee, Deposition of nitrogen-containing diamond-like carbon films on acrylic substrates by an ion beam process. *Vacuum* **74**, 531–538 (2004)
  61. R. Zarei Moghadam, H. Ahmadvand, M. Jannesari, Design and fabrication of multi-layers infrared antireflection coating consisting of ZnS and Ge on ZnS substrate. *Infrared Phys. Technol.* **75**, 18–21 (2016)
  62. C. Forsich, D. Heim, T. Mueller, Influence of the deposition temperature on mechanical and tribological properties of a-C:H:Si coatings on nitrided and postoxidized steel deposited by DC-PACVD. *Surf. Coat. Technol.* **203**, 521–525 (2008)
  63. C. Zeng, Q. Chen, M. Xu, S. Deng, Y. Luo, T. Wu, Enhancement of mechanical, tribological and morphological properties of nitrogenated diamond-like carbon films by gradient nitrogen doping. *Diam. Relat. Mater.* **76**, 132–140 (2017)
  64. N. Kaushik, P. Sharma, M. Nishijima, A. Makino, M. Esashi, S. Tanaka, Structural, mechanical and optical properties of thin films deposited from a graphitic carbon nitride target. *Diam. Relat. Mater.* **66**, 149–156 (2016)
  65. N. Dwivedi, S. Kumar, Nanoindentation testing on copper/diamond-like carbon bi-layer films. *Curr. Appl. Phys.* **12**, 247–253 (2012)
  66. S. Kumar, N. Dwivedi, C. Rauthan, Investigation of radio frequency plasma for the growth of diamond like carbon films. *Phys. Plasmas* **19**, 033515 (2012)

**Publisher's Note** Springer Nature remains neutral with regard to jurisdictional claims in published maps and institutional affiliations.